ELSEVIER

Journal of Fluids and Structures 23 (2007) 429–445

JOURNAL OF
FLUIDS AND
STRUCTURES

www.elsevier.com/locate/jfs

A new time-domain drag description and its influence on the dynamic behaviour of a cantilever pipe conveying fluid

G.L. Kuiper*, A.V. Metrikine, J.A. Battjes

Faculty of Civil Engineering and Geosciences, Delft University of Technology, Stevinweg 1 2628 CN Delft, The Netherlands

Received 19 January 2006; accepted 30 September 2006

Abstract

Studying dynamic stability of a vertically suspended, fully submerged pipe conveying fluid upwards, researchers have found a contradiction between theoretical predictions and experiments. Experiments did not show any instability, while theory predicts instability at infinitesimally low fluid velocities for a pipe without dissipation mechanisms. To explain this contradiction, in 2005 Païdoussis and co-workers postulated a new description of the boundary condition at the free end of the pipe. Subject to this boundary condition the pipe is predicted to become unstable by divergence (stable node to saddle bifurcation) at a velocity higher than yet achieved in experiments. In this paper, it is shown that a realistic description of hydrodynamic drag in combination with conventional boundary conditions might result in even higher critical velocity, and hence, this could also be an explanation of the contradiction. The description of the hydrodynamic drag is based on experimental data available in literature. This data has been obtained by experimenting with submerged rigid cylinders. To make it applicable to flexible pipes, a key step is undertaken in this paper to translate the data from the frequency domain to the time domain. Using the time-domain description of the hydrodynamic drag in combination with the conventional boundary conditions at the free end, it is shown that the pipe becomes unstable by flutter (stable focus to unstable focus bifurcation) at a critical velocity, which is much higher than that attainable in small-scale experiments. For fluid velocities exceeding the critical one, the pipe motion reaches a steady oscillation of finite amplitude, i.e. a stable limit cycle.

Keywords: Cantilever pipe; Stability; Hydrodynamic drag; Fluid–structure interaction; Flexible cylinder

---

1. Introduction

Submerged, cantilever pipes conveying fluid recently had a revival of practical interest. A new concept was developed of liquefying natural gas on a barge offshore. This process requires large volumes of cooling water. Designs were made for pipes suspended from the floating barge for the conveyance of cooling water. These pipes, referred to as free-hanging risers, have an unconstrained tip (lower end) and convey fluid upwards. Instability (vibration in the bending mode) of these risers should be avoided.

In recent years, different theories have been developed to predict stability of submerged, cantilever pipes conveying fluid upwards. It was first thought that once all dissipation mechanisms are neglected, the cantilever pipe loses stability

---

*Corresponding author. Tel.: +31 015 2784671; fax: +31 015 2785767.
E-mail address: G.L.Kuiper@tudelft.nl (G.L. Kuiper).

0889-9746/$ - see front matter © 2006 Elsevier Ltd. All rights reserved.
doi:10.1016/j.jfluidstructs.2006.09.007

at infinitesimal fluid velocities (Païdoussis and Luu, 1985). In this paper, the conventional boundary conditions were used, i.e. the bending moment and the shear force are assumed to be zero at the free end. Physically, this means that neither the direction nor the absolute value of the momentum of the fluid changes direction as the fluid enters the pipe, implying that the average velocity of the fluid is tangential to the *deflected* pipe.

Using these boundary conditions and employing the method proposed by Lee and Mote (1997), one can prove that irrespective of the wave frequency, at the upstream free end and at the downstream fixed end of a tensioned cantilever pipe aspirating water, there is a positive energy flux into the pipe during wave reflection from both ends. The positive energy flux at both boundaries implies that, in the absence of hydrodynamic drag, instability occurs at infinitely small fluid velocities. However, this is in contrast with experiments, which did not show such instability.

An attempt to explain this contradiction was made by Païdoussis (1999), suggesting that the theoretical prediction is wrong because of an improper description of the negative pressurization of water at the inlet of the pipe. However, Kuiper and Metrikine (2005) showed that this pressurization influences the stability only slightly. In addition, they showed, using a linearized drag description, that the external hydrodynamic drag is the major stabilizing factor, which prohibits the pipe instability at low flow speeds.

In reaction to this paper, Païdoussis et al. (2005) postulated several new descriptions of the boundary condition for the balance of the shear forces at the free end of the pipe. Their basic description of the boundary condition assumes that the inflow remains substantially tangential to the *undeflected* pipe. Using this boundary description the pipe is predicted to become unstable by divergence at a high fluid velocity, which has not yet been reached in experiments. Alternative variants of this boundary condition were also discussed and analysed by varying the assumptions concerning depressurization, tension and inflow direction. The main difference between all variants of the boundary condition presented by Païdoussis et al. (2005) and the conventional boundary condition is that the former assume that the fluid momentum changes direction as the fluid enters the pipe, whereas the latter considers this momentum to remain unchanged.

The correct description of the flow field in the vicinity of the tip is obviously of great importance for the stability of the pipe conveying fluid. To keep the comparison clean, in this paper we only analyse the two extreme boundary conditions for the balance of the shear forces at the free end. One is the conventional boundary condition which assumes an averaged inflow direction tangential to the deflected pipe. The other is the basic model of the boundary condition postulated by Païdoussis et al. (2005), which assumes an averaged inflow direction tangential to the undeflected pipe.

In agreement with Païdoussis et al. (2005), we think that the averaged inflow direction is tangential neither to the deflected pipe end nor to the undeflected pipe end, but that the angle between the pipe and the inflow varies in time between these two bounds. However, we think that reality is closer to the conventional boundary condition than to the recently proposed one. Using the travelling wave method for the situation in between these two extremes (Lee and Mote, 1997) it can be proven theoretically that the energy gain at the downstream fixed end is greater than the energy loss at the upstream end. Hence, in the absence of damping, the tensioned cantilever pipe model loses stability at infinitesimal fluid velocities. By adding a linear, external damping Kuiper and Metrikine (2005) showed that using the conventional boundary conditions the critical velocity corresponding to the instability onset is strongly influenced by this damping. Since the damping force employed by Kuiper and Metrikine (2005) was not based on experiments, no quantitative comparison of the critical velocity could be made with measurements. Note that in the above paper an extensive parametric study of the linearized drag on the critical velocity has been presented.

The aim of this paper is twofold, namely to predict quantitatively the onset of instability and the amplitude of the steady-state vibrations using physically realistic drag values. The onset of instability corresponds to infinitesimal deflections of the pipe and, therefore, to the laminar regime of the flow around the pipe. In this regime, the drag is proportional to the pipe velocity. The proportionality coefficient is realistically quantified in this paper using experimental data available in literature. The steady-state vibrations of the pipe correspond to larger deflections and velocities of the pipe, which cause the flow to separate from the pipe. In this turbulent regime the drag has a quadratic dependence on the transverse velocity of the pipe. This dependence is also quantified in this paper using experimental data.

This paper is structured as follows. In Section 2, a linearized equation of motion is presented of a submerged, free-hanging riser conveying fluid, and the main assumptions are discussed. Using Argand diagrams, the stability of the linearized system, using different boundary conditions at the free end, is analysed in Section 3. Section 4 is devoted to a time-domain description of hydrodynamic drag. The approach is to transform experimentally obtained frequency- and amplitude-dependencies of hydrodynamic drag to the time domain. The newly obtained drag description is used in Section 5 to study both the instability and the amplitude of the steady-state pipe vibrations. In this section, the conventional boundary conditions at the inlet are used. Employing the Galerkin's mode decomposition method it is shown that the theoretically computed critical fluid velocity is much higher than the fluid speeds attainable in the experiments with free hanging pipes aspirating water, and hence, it is not surprising that experiments did not show any instability.

2. Assumptions and equation of motion

The system under consideration is an initially straight, submerged, fluid-conveying pipe of finite length as sketched in Fig. 1. It is assumed that the pipe moves only in the plane that is depicted in this figure and performs small vibrations about the equilibrium configuration. The pipe is considered to be slender, its lateral deflection $w(z,t)$ to be small compared to the length of the pipe, and the vibrations be of a low frequency, so that the Euler–Bernoulli theory is applicable for description of the pipe dynamic bending. Due to gravity and internal fluid resistance the axial tension in the pipe $T_r(z)$ is a linear function of depth,

$$T_r(z) = \rho_r A_r g(L - z) - \rho_f A_r g L - \rho_f A_i \frac{f}{D_i}\frac{u_f^2}{2}(L - z), \tag{1}$$

with ρ_r and ρ_f the mass densities of the pipe material and the fluid, respectively, A_r the cross-sectional area of the pipe wall, A_i the internal cross-sectional area of the pipe, g the gravity acceleration, L the length of the pipe, D_i the inner diameter of the pipe, u_f the fluid velocity, and f the resistance coefficient of Darcy–Weisbach. The fluid outside the pipe is considered as still water. The internal fluid flow is approximated as a plug flow, i.e. as if it were an infinitely flexible rod travelling through the pipe, all points of the fluid having a velocity u_f relative to the pipe (directed upward). With these assumptions, the equation that governs the horizontal motion of a differential element of the pipe can be written as

$$\begin{aligned} &EI\frac{\partial^4 w}{\partial z^4} - \frac{\partial}{\partial z}\left(T_r(z)\frac{\partial w}{\partial z}\right) + \rho_f A_i\left(u_f^2\frac{\partial^2 w}{\partial z^2} - 2u_f\frac{\partial^2 w}{\partial z \partial t} + \frac{\partial^2 w}{\partial t^2}\right) \\ &\quad - \frac{\partial}{\partial z}\left((A_e p_e(z) - A_i p_i(z))\frac{\partial w}{\partial z}\right) + \rho_r A_r\frac{\partial^2 w}{\partial t^2} = f(z,t), \end{aligned} \tag{2}$$

with $w(z,t)$ the horizontal pipe displacement, z the coordinate along the pipe (directed downward), t the time, EI the bending stiffness of the pipe, A_e the external cross-sectional area of the pipe, $p_i(z)$ and $p_e(z)$ the water pressures inside and outside the pipe, respectively, $f(z,t)$ the normal dynamic reaction of the surrounding water on the pipe element. The external pressure is considered hydrostatic, while for the internal pressure the following expression is assumed:

$$p_i(z) = \rho_f g z - \rho_f\frac{u_f^2}{2} - \alpha_e\rho_f\frac{u_f^2}{2} - \rho_f\frac{f}{D_i}\frac{u_f^2}{2}(L - z), \tag{3}$$

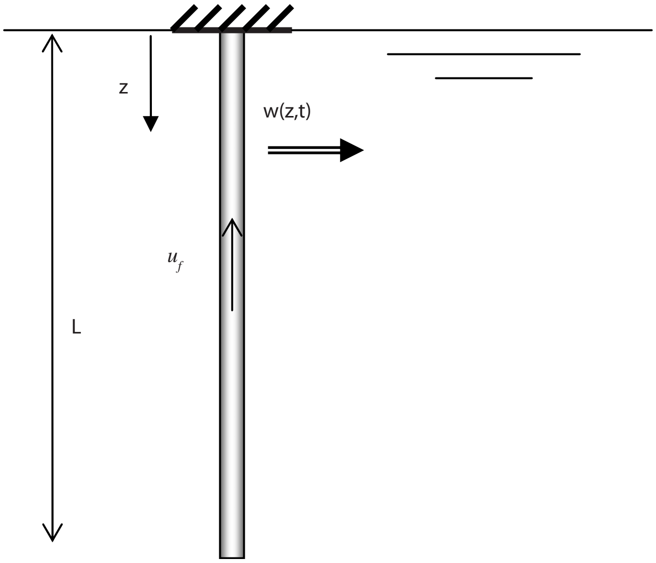

Fig. 1. Sketch of a submerged riser conveying fluid.

where α_e is the energy loss coefficient at the inlet. The four terms at the right-hand side represent, respectively, the hydrostatic pressure, the pressure drop due to the fluid speed, the pressure loss at the inlet and the pressure loss due to wall friction. Kuiper and Metrikine (2005) showed that the second and third terms have only a minor influence on the stability of the pipe, and hence, these terms are hereinafter disregarded.

The dynamic reaction of the surrounding water on the pipe, $f(z,t)$, is assumed to be a superposition of an inertia force $f_{in}(z,t)$ and a drag $f_d(z,t)$. The inertia force depends only on the acceleration of the pipe, since the surrounding fluid is considered here as still water. In this section, the description of the drag force is highly simplified assuming it in the form of a viscous damping (Païdoussis, 1998). In Section 4, a more realistic description of the drag is incorporated. The expression for the total force $f(z,t)$, used in this section, reads

$$f(z,t) = f_{in}(z,t) + f_d(z,t) = -\rho_f A_e C_a \frac{\partial^2 w}{\partial t^2} - \frac{1}{2}\rho_f D_o C_d^* \frac{\partial w}{\partial t}, \tag{4}$$

where D_o is the outer diameter of the pipe, C_a the added mass coefficient and C_d^* the adapted drag coefficient, with the dimension of velocity. Combining Eqs. (2)–(4), the resulting equation of motion for a pipe conveying fluid can be written as

$$EI\frac{\partial^4 w}{\partial z^4} - \frac{\partial}{\partial z}\left(T_e(z)\frac{\partial w}{\partial z}\right) - 2m_f u_f \frac{\partial^2 w}{\partial z \partial t} + m_f u_f^2 \frac{\partial^2 w}{\partial z^2} + M\frac{\partial^2 w}{\partial t^2} + \frac{1}{2}\rho_f D_o C_d^* \frac{\partial w}{\partial t} = 0, \tag{5}$$

in which

$$M = m_r + m_f + \rho_f A_e C_a, \quad T_e(z) = A_r g(\rho_r - \rho_f)(L - z).$$

The conventional boundary conditions at the ends of the submerged, suspended pipe are given as (Païdoussis, 1998, 1999; Kuiper and Metrikine, 2005)

$$w(z,t) = 0 \quad \text{and} \quad \frac{\partial w(z,t)}{\partial t} = 0 \quad \text{at } z = 0, \quad \frac{\partial^2 w(z,t)}{\partial z^2} = 0 \quad \text{and} \quad \frac{\partial^3 w(z,t)}{\partial z^3} = 0 \quad \text{at } z = L. \tag{6}$$

The boundary conditions at the lower end assume a zero bending moment and a zero shear force. In a recent paper, Païdoussis et al. (2005) argued that the force balance at the free end should be described not by the last equation of Eq. (6) but by the following relationship:

$$EI\frac{\partial^3 w(z,t)}{\partial z^3} - m_f u_f\left(\frac{\partial w(z,t)}{\partial t} - u_f\frac{\partial w(z,t)}{\partial z}\right) = 0 \quad \text{at } z = L. \tag{7}$$

Further to this description of the balance of shear forces, they discussed several other variants accounting for various depressurization, tensioning effects and direction of inflow. However, all their variants contain the term $m_f u_f(\partial w/\partial t)$, which is absent in the conventional boundary condition. This term cancels the effect of the Coriolis force in the equation of motion, insofar as the calculation of the energy gain at the boundaries is concerned. The new boundary condition (7) is based on the assumption that the momentum of the fluid changes as the fluid enters the pipe, i.e. the averaged fluid velocity changes direction, whereas the conventional boundary condition (6) presumes that the momentum remains unchanged. Using the new boundary condition, Païdoussis et al. (2005) explain that the pipe cannot become unstable at small fluid velocities since the total (over a period of vibrations) averaged amount of energy of the system remains constant. In this paper, the two extreme boundary conditions for the balance of the shear forces, (6) and (7), will be addressed.

Introducing the following dimensionless variables and parameters:

$$\eta = w/L, \ \xi = z/L, \ \tau = t\sqrt{EI/M}/L^2, \ \alpha = A_r g(\rho_r - \rho_f)L^3/EI,$$
$$\beta = \sqrt{m_f/M}, \ U = u_f L\sqrt{m_f/EI}, \ \gamma^* = \rho_f D_o C_d^* L^2 \Big/ \left(2\sqrt{MEI}\right),$$

the equation of pipe motion, Eq. (5), is rewritten as

$$\frac{\partial^4 \eta}{\partial \xi^4} - \alpha\frac{\partial}{\partial \xi}\left((1-\xi)\frac{\partial \eta}{\partial \xi}\right) - 2\beta U\frac{\partial^2 \eta}{\partial \xi \partial \tau} + U^2\frac{\partial^2 \eta}{\partial \xi^2} + \frac{\partial^2 \eta}{\partial \tau^2} + \gamma^*\frac{\partial \eta}{\partial \tau} = 0. \tag{8}$$

The four conventional boundary conditions (6) and the proposed balance of forces at the free end (7) (Païdoussis et al., 2005) are written in dimensionless form as, respectively:

$$\eta(\xi,\tau)=0 \quad \text{and} \quad \frac{\partial\eta(\xi,\tau)}{\partial\xi}=0 \quad \text{at } \xi=0, \quad \frac{\partial^2\eta(\xi,\tau)}{\partial\xi^2}=0 \quad \text{and} \quad \frac{\partial^3\eta(\xi,\tau)}{\partial\xi^3}=0 \quad \text{at } \xi=1, \tag{9}$$

$$\frac{\partial^3\eta(\xi,\tau)}{\partial\xi^3}-U\left(\beta\,\frac{\partial\eta(\xi,\tau)}{\partial\tau}-U\,\frac{\partial\eta(\xi,\tau)}{\partial\xi}\right)=0 \quad \text{at } \xi=1. \tag{10}$$

3. Stability of a pipe conveying fluid in the linear approximation

The dynamic stability of a linear system is determined by its eigenfrequencies. To find these, the displacement of the pipe can be sought for in the following form:

$$\eta(\xi,\tau)=W(\xi)e^{i\omega\tau},$$

where ω is the dimensionless, generally complex frequency. Hence, the system is stable if the imaginary part of all eigenfrequencies is positive, and unstable if at least one eigenfrequency has a negative imaginary part. The most common way to analyse the eigenfrequencies is to make use of an Argand diagram. In this diagram, the real and imaginary parts of the natural frequency ω are plotted parametrically, as they depend on one of the system parameters. Normally, the flow velocity u_f is used as such a parameter. In this section, along with u_f, the hydrodynamic drag is employed as the parameter to plot a part of the Argand diagram.

For the equation of motion of the free-hanging pipe, Eq. (8), with the conventional boundary conditions (9), the analysis and the results have been thoroughly discussed by Kuiper and Metrikine (2005). It was found that the stability of the pipe in this case depends strongly on the hydrodynamic drag. In the absence of the linearized drag the system

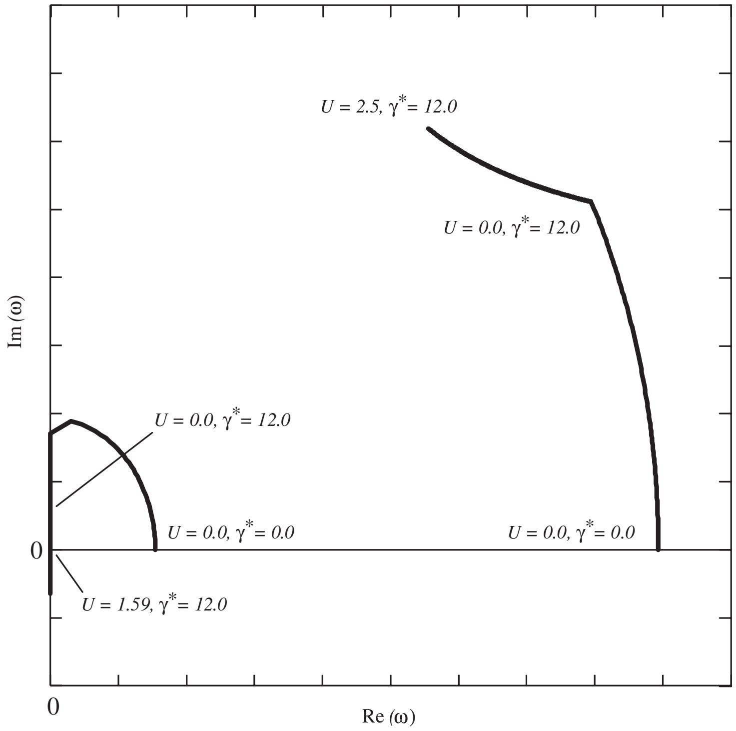

Fig. 2. Argand diagram with the first two loci. The pipe becomes unstable by divergence at $U = 1.59$ using the parameters of Table 1 and the new proposed boundary condition, Eq. (10).

Table 1
Parameters used as base case

E	$1.00 \times 10^9\,\mathrm{N/m^2}$	ρ_f	$1.00 \times 10^3\,\mathrm{kg/m^3}$
L	$2.00\,\mathrm{m}$	ρ_r	$1.20\,10^3\,\mathrm{kg/m^3}$
D_o	$3.00 \times 10^{-2}\,\mathrm{m}$	C_a	1.00
D_i	$2.60 \times 10^{-2}\,\mathrm{m}$	v	$1.00 \times 10^{-6}\,\mathrm{m^2/s}$

becomes unstable at infinitesimal fluid velocity. By increasing the adapted drag coefficient, the fluid velocity for which the transition occurs from stable to unstable behaviour is increased significantly. The pipe becomes unstable by flutter (stable focus to unstable focus bifurcation).

A completely different picture appears for the equation of motion of the free-hanging pipe, Eq. (8), in combination with the new boundary condition (10) of Païdoussis et al. (2005). As can be seen in the Argand diagram in Fig. 2 the pipe becomes unstable by divergence (stable node to saddle bifurcation). Only the first two eigenfrequencies are plotted for an adapted drag coefficient C_d^* of 1.0 m/s and using the parameters given in Table 1. These parameters simulate a flexible, plastic pipe of 2.0 m length fully submerged in water. Fig. 2 shows that the path of the first natural frequency intersects the real ω-axis first for increasing flow velocity u_f. As expected, the amount of hydrodynamic drag has no influence on the fluid velocity for a system which becomes unstable by divergence. This means that, even in the absence of the drag, a relatively high fluid velocity should be achieved to render the pipe unstable. For the parameters in Table 1, the dimensionless critical velocity is equal to $U_{\mathrm{crit}} = 1.59$, corresponding to $u_{f,\mathrm{crit}} = 4.53\,\mathrm{m/s}$.

As noted in Section 1, the spatially averaged fluid inflow at the free end is probably tangential neither to the deflected nor to the undeflected pipe. For a cantilever pipe model with average inlet flow between these two bounds, the stability will strongly depend on the amount of hydrodynamic drag. To assess the onset of instability and the amplitude of the pipe motion after the onset, more realistic drag description based on experiments should be incorporated into the model.

4. Hydrodynamic drag on flexible cylinders

4.1. Existing experiments

In order to obtain reliable predictions of the dynamic behaviour of submerged pipes, a drag description based on previous experiments is used. For measuring hydrodynamic drag acting on a pipe section in still water, a straight rigid cylinder is used conventionally. In literature, three test set-ups have been described:

(i) a water tank where the cylinder is subjected to forced oscillations at a constant frequency [e.g. Chaplin and Subbiah (1998)],
(ii) a water tank where a cylinder undergoes decaying oscillations following an initial displacement [e.g. Bearman and Russell (1996)],
(iii) a U-shaped water tunnel where the flow oscillates about a cylinder at a constant frequency [e.g. Sarpkaya (1986)].

The drag on a rigid cylinder oscillating in still water is characterized by the Stokes parameter β and the Keulegan–Carpenter number KC defined as, respectively:

$$\beta = \frac{D_o^2}{vT} \quad \text{and} \quad \mathrm{KC} = \frac{2\pi\hat{x}}{D_o}, \tag{11}$$

where $\hat{x}$ is the amplitude of the cylinder displacement, T the period of oscillation and υ the kinematic viscosity of the water.

At low values of KC ($\mathrm{KC} < 0.1$), i.e. small displacement-to-diameter ratios, the flow remains predominantly attached to the cylinder, and the drag is due to viscous forces in a thin boundary layer attached to the body. For a circular cylinder oscillating harmonically at small amplitudes in water otherwise at rest, the damping is conveniently expressed as proposed by Stokes (1851) and later extended by Wang (1968). For large values of β ($\beta > 10^5$), this damping is approximately proportional to the velocity of the cylinder, $\mathrm{d}x/\mathrm{d}t$. Its value per unit length is given as

$$F_{\text{Stokes}} = 2\pi^{3/2}\rho_f \upsilon\sqrt{\beta}\,\frac{\mathrm{d}x}{\mathrm{d}t} = 2\pi^{3/2}\,\frac{\rho_f D_o\sqrt{\upsilon}}{\sqrt{T}}\,\frac{\mathrm{d}x}{\mathrm{d}t}, \tag{12}$$

At larger values of KC ($\mathrm{KC}>0.1$), the flow separates from the pipe, forming a turbulent wake behind the body. In this turbulent regime, the drag has a quadratic dependence on the transverse velocity of the pipe. In this case, the instantaneous force acting on the cylinder per unit length is normally expressed as the often-used Morison damping:

$$F_{\text{Morison}} = \frac{1}{2}\rho_f D_o C_d\,\frac{\mathrm{d}x}{\mathrm{d}t}\left|\frac{\mathrm{d}x}{\mathrm{d}t}\right|. \tag{13}$$

Conventionally, even the linear Stokes damping is expressed in terms of a quadratic dependence on velocity, although the instantaneous force is not proportional to the square of the instantaneous velocity, as the use of the Morison expression normally suggests. In order to do this, the nonlinear drag force is rewritten as a Fourier series, under the assumption that the velocity has a sinusoidal character

$$\frac{1}{2}\rho_f D_o C_d(\hat{x}\omega)^2\cos(\omega t)|\cos(\omega t)| \approx \frac{1}{2}\rho_f D_o C_d(\hat{x}\omega)^2\left(\frac{8}{3\pi}\cos(\omega t) + \frac{1}{2}\cos(2\omega t) + \ldots\right),$$

where $\omega = 2\pi/T$. Taking only the first Fourier term into account, i.e. neglecting the higher harmonics, the hydrodynamic drag coefficient C_d of the Morison damping at low KC is then given by

$$C_d = \frac{3\pi^3}{2\sqrt{\pi}}\,\frac{1}{\mathrm{KC}\sqrt{\beta}}. \tag{14}$$

The inverse dependence of C_d on KC compensates for expressing a linear drag through a quadratic dependence of velocity.

Experimental studies of hydrodynamic drag on a cylinder oscillating in still water at small amplitudes and large Stokes parameters ($\beta>6\times10^4$) have been carried out by, among others, Bearman and Russell (1996), Chaplin and Subbiah (1998) and Chaplin (2000). These experiments for low Keulegan–Carpenter numbers show a near doubling of the C_d value in comparison with the value predicted by the Stokes–Wang theoretical analysis, Eq. (14). Sarpkaya (2001) attempted to find a reason for the deviation of the measured values from the Stokes–Wang laminar flow theory, however he found good explanation for the doubling of the drag.

In the turbulent regime, in which the displacement amplitudes are relatively large ($\mathrm{KC}>0.1$), Bearman and Russell (1996) argue that a contribution to C_d of 0.08KC can be expected. They proposed a semi-empirical formula for the total drag coefficient of the form

$$C_d = \frac{\zeta_1}{\mathrm{KC}\sqrt{\beta}} + \zeta_2\,\mathrm{KC} = \frac{\zeta_1}{\sqrt{\mathrm{Re}\,\mathrm{KC}}} + \zeta_2\,\mathrm{KC} \tag{15}$$

with $\zeta_1 = 55$ and $\zeta_2 = 0.08$. Especially for very small KC numbers this formula predicts the drag coefficient in good agreement with the experiments. Expression (15) is only valid for smooth cylinders and is measured in the abovementioned experiments for a KC number of 0.3. For smaller values of the Stokes parameter ($\beta<3\times10^4$) experiments have been conducted for higher Keulegan–Carpenter numbers up to 12 (Justesen, 1988; Rodenbusch and Kallstrom, 1986). Although the same trend for C_d is observed in all the results, there is an appreciable scatter in the data for the higher Keulegan–Carpenter numbers. Sarpkaya (2001) observed that, with increasing Keulegan–Carpenter number, regular (Honji-instabilities) and irregular mushroom-shaped vortices, arise first, followed by turbulence, separation and vortex shedding. Due to the stochastic behaviour of vortices, a large scatter was observed in the experimental results for larger *KC*-values. Nevertheless, we assume that formula (15) is valid for Keulegan–Carpenter numbers up to 8. The semi-empirical formula, Eq. (15), has been plotted in Fig. 3 for two values of the Stokes parameter. For rough cylinders the drag coefficient should be increased, depending on the roughness [see e.g., Bearman and Mackwood (1992), Chaplin and Subbiah (1998)].

4.2. Experimental drag force applicable to flexible pipes

In order to use Eq. (15) for prediction of the dynamic behaviour of a flexible pipe in the time domain, an iterative procedure is required, because through KC the drag depends on the unknown displacement amplitude and period. Such procedure is straightforward if the pipe vibrates in a single-mode regime. However, flexible pipes often exhibit multi-mode vibrations. In this case, the motion of each section of the pipe is approximately decomposable into a number of

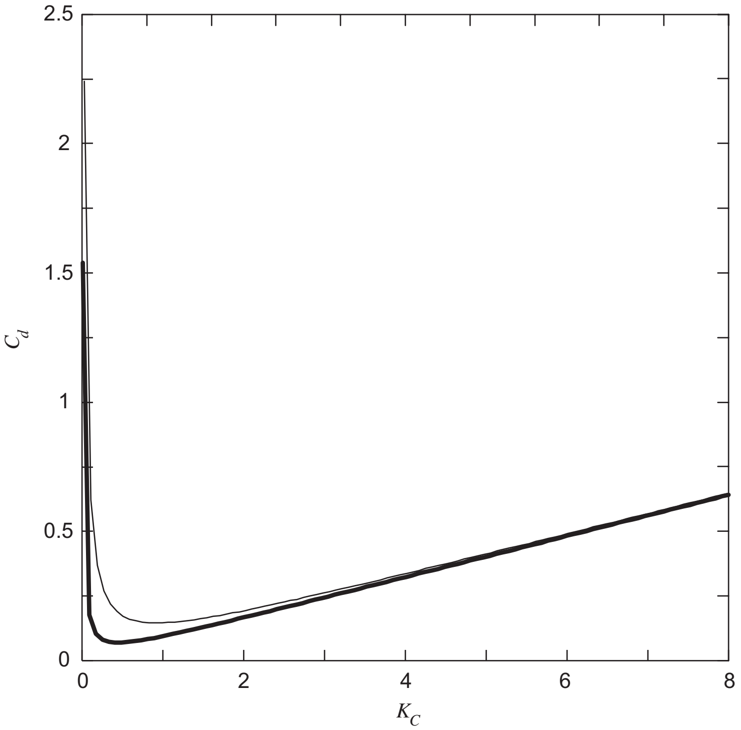

Fig. 3. Drag coefficient according to Eq. (15) versus Keulegan–Carpenter number for $\beta = 670.000$ (regular line) and $\beta = 1.277.000$ (bold line).

harmonic vibrations that have different amplitudes. This makes the iterative procedure cumbersome and not necessarily convergent. Therefore, in this paper, an alternative approach is proposed for description of the drag coefficient. Instead of using the frequency domain representation of the drag coefficient, Eq. (15), a time-domain expression for the drag is proposed. Using the time domain expression, vibrations of a flexible pipe can be studied by any conventional time-domain method (FEM, finite difference, Galerkin method, etc.) without employing an iterative procedure.

The idea is to reconstruct a time domain drag coefficient on the basis of Eq. (15), which should result in a similar dynamic pipe response. A rigid, elastically mounted cylinder is externally excited at the resonance frequency ω_e. The resonance excitation is assumed because it is most sensitive to damping. The predictions obtained using the frequency and time-domain descriptions are compared to each other requiring that the displacement amplitudes are the same for the same external force. The following equation of motion describes oscillations of this cylinder in water, provided that the Morison's formula is applicable:

$$\frac{\mathrm{d}^2x}{\mathrm{d}t^2} + \frac{\rho_f DlC_d}{2m}\frac{\mathrm{d}x}{\mathrm{d}t}\left|\frac{\mathrm{d}x}{\mathrm{d}t}\right| + \omega_e^2 x = \frac{F}{m}\sin(\omega_e t), \tag{16}$$

where x is the displacement of the cylinder, l the length of the rigid cylinder, m the mass of the cylinder plus the added mass and F the amplitude of the external force. The Stokes parameter β and the resonance frequency ω_e are related to each other, as indicated by Eq. (11):

$$\beta = \frac{D_o^2\omega_e}{2\pi\nu}. \tag{17}$$

Owing to the oscillatory force, the cylinder reaches a periodic motion, and its amplitude can be characterized by the Keulegan–Carpenter number. Starting with the frequency domain description of the drag coefficient, Eq. (15), the drag force reads

$$F_{\mathrm{drag}} = \frac{\rho_f D_o l}{2}\left(\frac{\zeta_1\sqrt{\nu T}}{2\pi\hat{x}} + \zeta_2\frac{2\pi}{D_o}\hat{x}\right)\frac{\mathrm{d}x}{\mathrm{d}t}\left|\frac{\mathrm{d}x}{\mathrm{d}t}\right|. \tag{18}$$

Using this drag force, the steady-state solution can be computed (using an iterative procedure) for a given external oscillatory force. This computation has been repeated for 20 amplitudes of the external force, so that the range of Keulegan–Carpenter numbers of our interest is covered ($0.01<\mathrm{KC}<8$). Besides, systems with three natural frequencies are considered, by using different values for the Stokes parameter ($\beta_1 = 6.700\times10^5$, $\beta_2 = 1.025\times10^6$, $\beta_3 = 1.277\times10^6$) according to Chaplin's experiments (2000).

The time-domain description of the drag coefficient should result in the same dynamic response of the rigid cylinder as it is loaded by the same force. As explained before, the hydrodynamic damping for small displacements ($\mathrm{KC}<0.1$) is caused by viscous effects apparent in a thin boundary layer attached to the pipe. This force is proportional to the velocity of the pipe. For larger displacements and velocities, the flow separates from the pipe, forming a turbulent wake behind the body, and the drag is proportional to the square of the pipe velocity. A superposition of these two contributions is proposed for the description of the drag force in the time domain:

$$F_{\mathrm{drag,new}} = D_o l\left(\frac{\mu}{D_o}A_1\frac{\mathrm{d}x}{\mathrm{d}t} + \frac{1}{2}\rho_f A_2\left|\frac{\mathrm{d}x}{\mathrm{d}t}\right|\frac{\mathrm{d}x}{\mathrm{d}t}\right), \tag{19}$$

where A_1 and A_2 are two unknown dimensionless constants and μ is the dynamic viscosity of the fluid ($\nu = \mu/\rho_f$).

According to Eq. (15), the drag coefficient increases with amplitude (for $\mathrm{KC}<8$), while Eq. (19) has a constant coefficient in front of the velocity-squared term. This suggests a cubic velocity dependence to capture this difference. However, it is not easy to get the dimensions of an additional cubic term correctly. Nor is it straightforward to link this term to the underlying physics. Speculating about this, we think that the cubic term should depend on the vortex shedding frequency. Unfortunately, the current available experiments do not give information about this. Therefore, we do not pursue this cubic velocity dependence of the drag. Note that this cubic term does not have an effect on the onset of instability, but only on the steady-state amplitude.

To find the unknown constants A_1 and A_2, Eq. (16) is rewritten using $F_{\mathrm{drag,new}}$:

$$\frac{\mathrm{d}^2x}{\mathrm{d}t^2} + D_o l\left(\frac{\mu}{D_o}A_1\frac{\mathrm{d}x}{\mathrm{d}t} + \frac{1}{2}\rho_f A_2\left|\frac{\mathrm{d}x}{\mathrm{d}t}\right|\frac{\mathrm{d}x}{\mathrm{d}t}\right) + \omega_e^2 x = \frac{F}{m}\sin(\omega_e t). \tag{20}$$

The steady-state solution of this equation is computed for the same 20 amplitudes and three frequencies of the external force as in the previous case. The two unknowns in Eq. (19), A_1 and A_2, should be chosen such that the differences between the results for the dynamic response of the cylinder corresponding to the descriptions of the drag

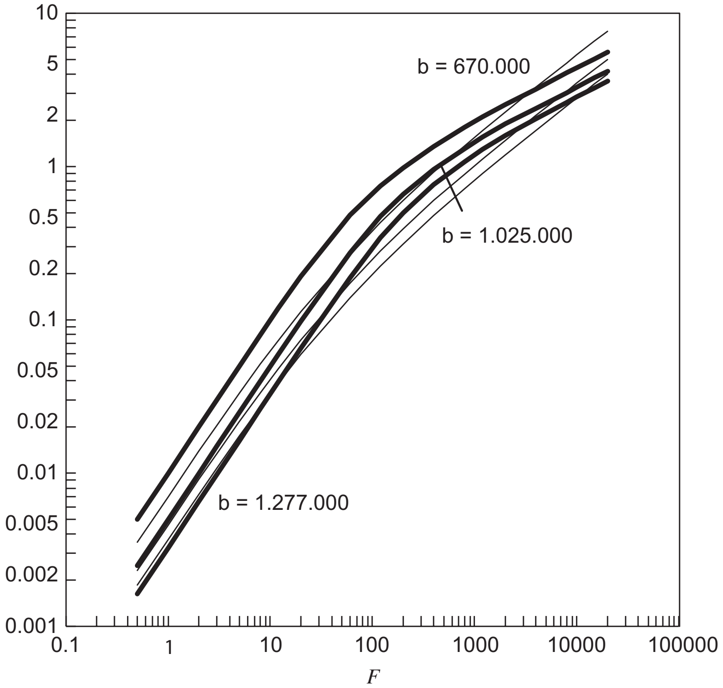

Fig. 4. Keulegan–Carpenter number versus external force for different Stokes parameters. Bold line: Eq. (18); regular line Eq. (19).

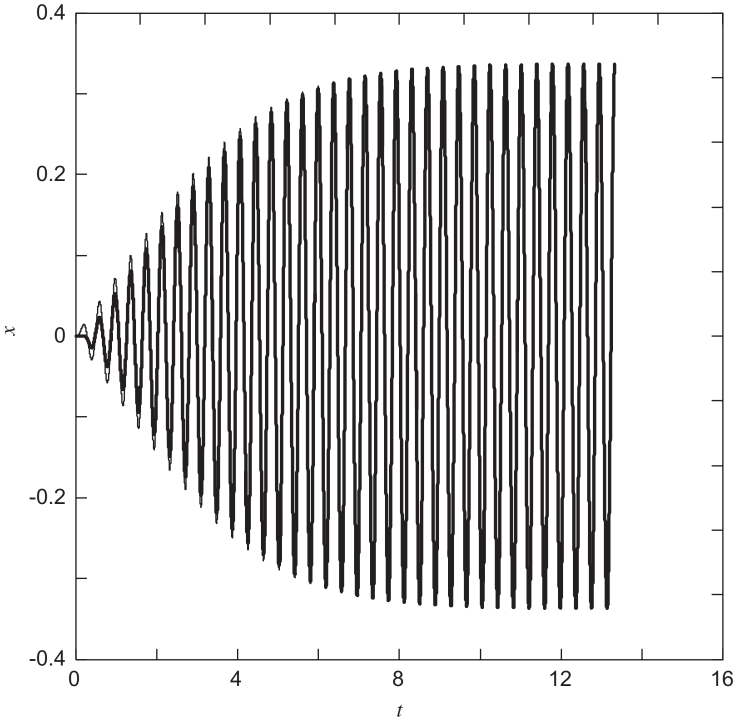

Fig. 5. Time series of a damped cylinder displacement subjected to an external oscillatory force using different drag coefficients, based on Eq. (18) (bold line) and based on Eq. (19) (regular line).

coefficient in the frequency domain and in the time domain are minimal in some sense. To achieve this, a procedure was applied to minimize the difference in KC-value (for each given F and β) in the steady-state motion for both drag descriptions by varying the unknowns A_1 and A_2. It was found that the smallest error in KC is obtained by choosing $A_1 = 27 \times 10^3$ and $A_2 = 0.24$. The KC-F dependence obtained with these values of A_1 and A_2 is shown in Fig. 4. The same parameters as in the experiments performed by Chaplin (2000) were used: $m = 4.08 \times 10^3\,\mathrm{kg}$, $D_o = 0.75\,\mathrm{m}$, $l = 4.29\,\mathrm{m}$, $\rho_f = 1.00 \times 10^3\,\mathrm{kg\,m^{-3}}$, $\nu = 1.14 \times 10^{-6}\,\mathrm{m^2\,s^{-1}}$.

The Keulegan–Carpenter number in the steady-state regime is plotted as a function of the amplitude of the external oscillatory force. The bold lines correspond to the drag according to Eq. (18), while the regular lines correspond to the new description of the drag, Eq. (19). As an example, the displacement in the time domain of a cylinder subject to the external oscillatory force with $F = 1.00 \times 10^5\,\mathrm{N}$ and $\beta = 1.277 \times 10^6$ is given in Fig. 5. In this figure, the two lines are plotted using the two different descriptions of the hydrodynamic drag.

As can be concluded from Figs. 4 and 5, the time-domain description can be considered to reproduce the hydrodynamic drag in reasonable accordance with the experiments in the range of KC up to 8. In Fig. 4, a difference in slope is observed for values of KC above 0.2. The reason for this deviation is that in expression (18) C_d has a cubic dependence on KC, while in expression (19) this dependence is quadratic. As noted, this difference does not affect the calculated onset of instability.

5. Stability of a pipe conveying fluid with nonlinear drag

In this section, the influence of the hydrodynamic drag on stability of a free-hanging pipe conveying fluid is investigated by using a nonlinear, time-domain description of the hydrodynamic drag, as derived in the previous section. At the free end, the conventional boundary conditions are used, Eq. (9). Only for these boundary conditions does the hydrodynamic drag have a significant effect on the onset of instability of the pipe. For the boundary conditions proposed by Païdoussis et al. (2005), Eq. (10), the results of Section 3 are applicable for prediction of the onset, as this is not affected by the hydrodynamic drag.

The equation of motion of the submerged pipe subjected to the nonlinear hydrodynamic drag reads

$$EI\,\frac{\partial^4 w}{\partial z^4}-\frac{\partial}{\partial z}\left(T_e(z)\frac{\partial w}{\partial z}\right)-2m_f u_f\,\frac{\partial^2 w}{\partial z\partial t}+m_f u_f^2\,\frac{\partial^2 w}{\partial z^2}+M\,\frac{\partial^2 w}{\partial t^2}+D_o\left(\frac{\mu}{D_o}A_1\,\frac{\partial w}{\partial t}+\frac{1}{2}\,\rho_f A_2\left|\frac{\partial w}{\partial t}\right|\frac{\partial w}{\partial t}\right)=0 \tag{21}$$

Using the dimensionless variables and parameters

$$\eta=w/L,\;\; \xi=z/L,\;\; \tau=t\sqrt{EI/M}\Big/L^2,\;\; \alpha=A_r g(\rho_r-\rho_f)L^3/EI,$$

$$\beta=\sqrt{m_f/M},\;\; U=u_f L\sqrt{m_f/EI},\;\; \varsigma=\mu L^2\Big/\sqrt{MEI},\;\; \gamma=\rho_f D_o L/(2M),$$

the equation of motion, Eq. (21) is rewritten as

$$\frac{\partial^4\eta}{\partial\xi^4}-\alpha\,\frac{\partial}{\partial\xi}\left((1-\xi)\frac{\partial\eta}{\partial\xi}\right)-2\beta U\,\frac{\partial^2\eta}{\partial\xi\partial\tau}+U^2\,\frac{\partial^2\eta}{\partial\xi^2}+\frac{\partial^2\eta}{\partial\tau^2}+\varsigma A_1\,\frac{\partial\eta}{\partial\tau}+\gamma A_2\left|\frac{\partial\eta}{\partial\tau}\right|\frac{\partial\eta}{\partial\tau}=0. \tag{22}$$

Note that the critical fluid velocity does not depend on the nonlinear term in Eq. (22). Therefore, the critical velocities predicted by Eq. (8) and Eq. (22) may differ due to a difference between γ^* and ζA_1. The advantage of using ζA_1 is that the numerical value of this coefficient is based on experimental data.

5.1. Galerkin method

Different methods (FEM, finite difference, etc.) are applicable for solving nonlinear partial differential Eq. (22). In this paper, we have chosen the Galerkin method, since it provides better insight in the physics of the dynamic stability of the pipe than the other time domain numerical methods. The Galerkin procedure is used to approximate the nonlinear partial differential equation by a finite set of coupled ordinary differential equations, with the solution expressed as

$$\eta(\xi,\tau)=\sum_{m=1}^{\infty}\phi_m(\xi)q_m(\tau), \tag{23}$$

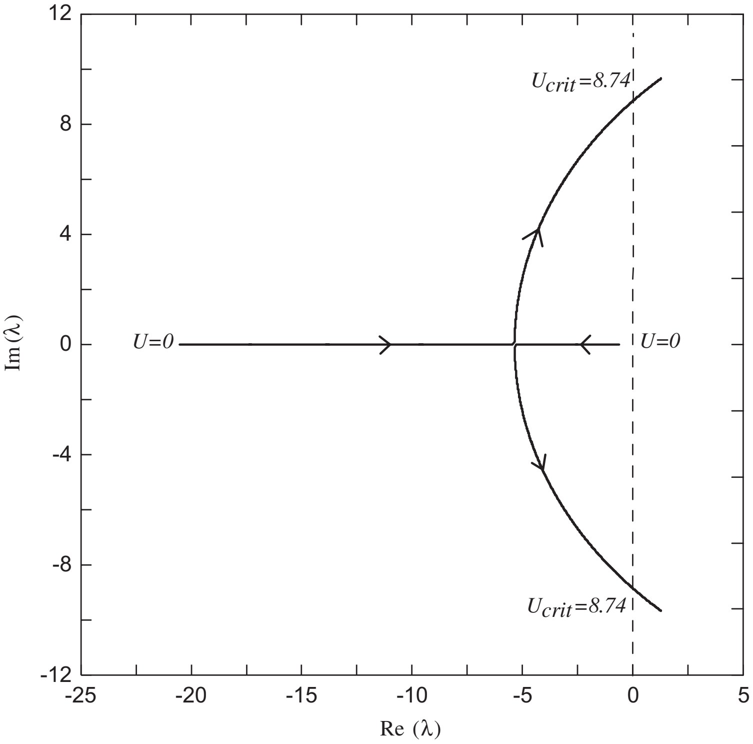

Fig. 6. Argand diagram of the complex eigenvalues for a one-mode Galerkin decomposition. The numerical value of U_{crit} is based on the parameters of Table 1.

where $q_m(\tau)$ are unknown time-dependent functions and $\phi_m(\xi)$ are space-dependent shape functions forming a complete set. The $\phi_m(\xi)$ are chosen as the eigenfunctions of the following operator:

$$\frac{\mathrm{d}^4}{\mathrm{d}\xi^4} - \alpha\frac{\mathrm{d}}{\mathrm{d}\xi}\left((1-\xi)\frac{\mathrm{d}}{\mathrm{d}\xi}\right) - \Omega_m^2 = 0 \tag{24}$$

satisfying the conventional boundary conditions, Eq. (9), where Ω_m are the corresponding eigenfrequencies. The functions $\phi_m(\xi)$ form a complete orthogonal set. The orthogonality condition is used to obtain the functions $q_n(\tau)$. Substituting Eq. (23) into Eq. (22), multiplying through by ϕ_n, and integrating over $\xi \in (0,1)$, it is found that

$$\frac{\mathrm{d}^2 q_n}{\mathrm{d}\tau^2} - 2\beta U \sum_{m=1}^{\infty} B_{mn}\frac{\mathrm{d}q_m}{\mathrm{d}\tau} + \Omega_n^2 q_n + U^2\sum_{m=1}^{\infty} C_{mn} q_m + \varsigma A_1\frac{\mathrm{d}q_n}{\mathrm{d}\tau} + \gamma A_2 \sum_{m=1}^{\infty}\sum_{l=1}^{\infty} D_{lmn}\left|\frac{\mathrm{d}q_l}{\mathrm{d}\tau}\right|\frac{\mathrm{d}q_m}{\mathrm{d}\tau} = 0, \tag{25}$$

where

$$B_{mn} = \int_0^1 \frac{\mathrm{d}\phi_m}{\mathrm{d}\xi}\phi_n\,\mathrm{d}\xi \Big/ \int_0^1 \phi_n^2\,\mathrm{d}\xi, \quad C_{mn} = \int_0^1 \frac{\mathrm{d}^2\phi_m}{\mathrm{d}\xi^2}\phi_n\,\mathrm{d}\xi \Big/ \int_0^1 \phi_n^2\,\mathrm{d}\xi,$$

$$D_{lmn} = \int_0^1 |\phi_l|\phi_m\phi_n\,\mathrm{d}\xi \Big/ \int_0^1 \phi_n^2\,\mathrm{d}\xi.$$

5.2. One-mode approximation

First, the results of the one-mode Galerkin approximation are shown (only the first mode is accounted for). This approximation is presented to explain the basic instability mechanisms of a cantilever pipe conveying fluid. In the next two sections, higher modes are taken into account to achieve higher accuracy. For the one-mode Galerkin

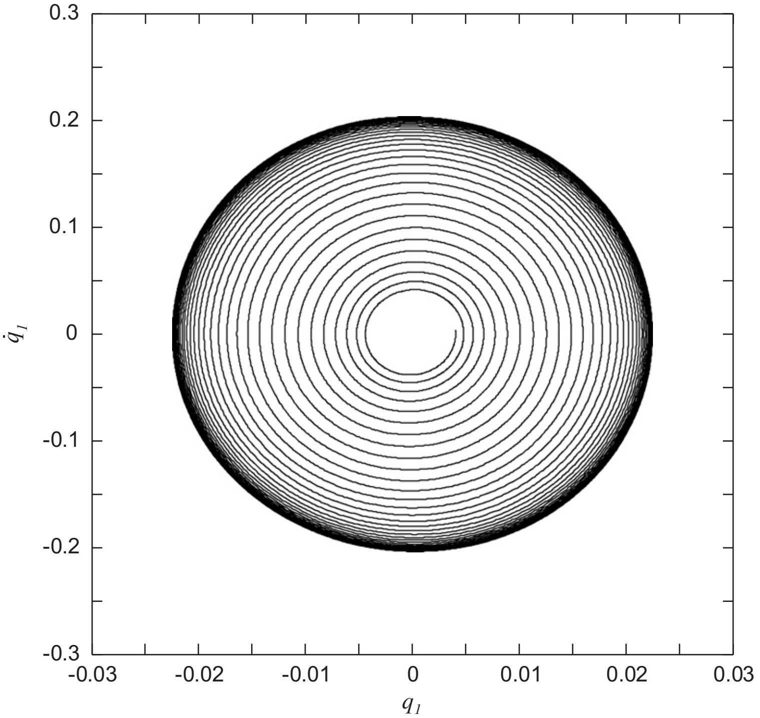

Fig. 7. Phase-plane for a fluid velocity exceeding the critical fluid velocity, showing a stable limit cycle.

approximation ($n = 1$), Eq. (25) can be written as two coupled first-order differential equations:

$$\begin{Bmatrix} \dot{q}_1 \\ \dot{p}_1 \end{Bmatrix} = \begin{bmatrix} 0 & 1 \\ -\Omega_1^2 - U^2 C_{11} & 2\beta U B_{11} - A_1 \varsigma \end{bmatrix} \begin{Bmatrix} q_1 \\ p_1 \end{Bmatrix} + f(p_1), \tag{26}$$

where $f(p_1)$ is a vector containing the nonlinear terms. This system has only one equilibrium point given by $q_1 = p_1 = 0$. The type of this equilibrium is found by linearizing Eq. (26) in the vicinity of this point. The complex eigenvalues λ are shown in the Argand diagram in Fig. 6 for varying flow velocity U. Note that the axes of this diagram represent the real and imaginary values of the eigenvalues λ instead of the eigenfrequencies ω, which was the case in Section 3 ($\lambda = \mathrm{i}\omega$). This change is made since it is more common in the field of nonlinear dynamics to work with eigenvalues.

The criterion for the instability to occur is that at least one of the eigenvalues has a positive real part. The one-mode system loses stability through the Hopf bifurcation, i.e. stable focus to unstable focus bifurcation, at a critical fluid velocity of

$$U_{\mathrm{crit}} = \frac{A_1 \varsigma}{2\beta B_{11}}. \tag{27}$$

Using the base case parameters as shown in Table 1, the dimensionless critical velocity of the simulated pipe is found as $U_{\mathrm{crit}} = 8.74$.

It is interesting to investigate which terms in the equation of motion (22) are responsible for the energy input. At the critical velocity, the energy of the system considered over one period remains constant since both eigenvalues λ are imaginary. For the energy analysis the equation of motion in this case can be written as

$$\eta(\xi, \tau) = \phi_1(\xi) q_1(\tau) = \phi_1(\xi) \hat{q}_1 \cos(\omega_1 \tau), \tag{28}$$

where $\hat{q}_1$ is the amplitude of the harmonic motion and $\omega_1 = \sqrt{\Omega_1^2 + U_{\mathrm{crit}}^2 C_{11}}$. The energy variation over one period of the motion is caused by the centrifugal force, the Coriolis force and the linear part of the hydrodynamic drag. The

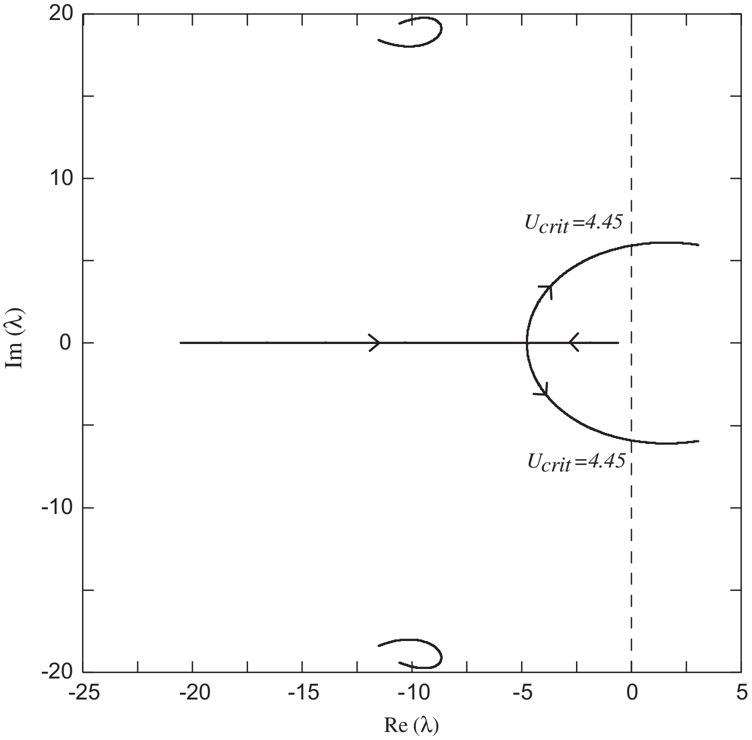

Fig. 8. Argand diagram of the complex eigenvalues for a two-mode Galerkin decomposition.

contributions of these forces to the energy loss read

$$\Delta E_{\text{Cent.}} = \int_0^T \int_0^1 F_{\text{Cent.}} \frac{\partial \eta}{\partial \tau} \, \mathrm{d}\xi \, \mathrm{d}\tau = U_{\text{crit}}^2 \int_0^T \int_0^1 \frac{\mathrm{d}^2 \phi_1}{\mathrm{d}\xi^2} \phi_1 q_1 \frac{dq_1}{d\tau} \, \mathrm{d}\xi \, \mathrm{d}\tau = 0, \tag{29}$$

$$\Delta E_{\text{Cor.}} = \int_0^T \int_0^1 F_{\text{Cor.}} \frac{\partial \eta}{\partial \tau} \, \mathrm{d}\xi \, \mathrm{d}\tau = -2\beta U_{\text{crit}} \int_0^T \int_0^1 \frac{\mathrm{d}\phi_1}{\mathrm{d}\xi} \phi_1 \left(\frac{\mathrm{d}q_1}{\mathrm{d}\tau} \right)^2 \mathrm{d}\xi \, \mathrm{d}\tau = -2\beta U_{\text{crit}} q_1^2 \pi \omega \int_0^1 \frac{\mathrm{d}\phi_1}{\mathrm{d}\xi} \phi_1 \, \mathrm{d}\xi, \tag{30}$$

$$\Delta E_{\text{DragL.}} = \int_0^T \int_0^1 F_{\text{DragL.}} \frac{\partial \eta}{\partial \tau} \, \mathrm{d}\xi \, \mathrm{d}\tau = \varsigma A_1 \int_0^T \int_0^1 \phi_1^2 \left(\frac{\mathrm{d}q_1}{\mathrm{d}\tau} \right)^2 \mathrm{d}\xi \, \mathrm{d}\tau = \varsigma A_1 q_1^2 \pi \omega \int_0^1 \phi_1^2 \, \mathrm{d}\xi. \tag{31}$$

The remaining terms in the equation of motion, Eq. (22), do not contribute to the energy variation over one period. As can be seen from Eq. (29) the centrifugal force does not contribute to the energy variation in the first mode approximation. From Eqs. (27), (30) and (31), it can be seen that the energy loss due to the linearized hydrodynamic drag is exactly equal to the energy gain due to the Coriolis force at the critical velocity.

In order to investigate the behaviour of the cantilever pipe conveying fluid after the onset of flutter, the nonlinear terms, as indicated in Eq. (26), have to be taken into account. The phase-plane for this system is shown in Fig. 7 for a fluid velocity exceeding the critical one, Eq. (27). One can see that the motion grows from sensibly zero to a steady oscillation of finite amplitude, i.e. to a stable limit cycle.

5.3. Two-mode approximation

A key difference between a one-mode and a two-mode Galerkin approximation is that in the latter case the possibility of mode interaction is accounted for. For the two-mode Galerkin approximation ($n = 2$), Eq. (25) can be rewritten in a system of four coupled first-order differential equations:

$$\begin{Bmatrix} \dot{q}_1 \\ \dot{p}_1 \\ \dot{q}_2 \\ \dot{p}_2 \end{Bmatrix} = \begin{bmatrix} 0 & 1 & 0 & 0 \\ -\Omega_1^2 - U^2 C_{11} & 2\beta U B_{11} - A_1 \varsigma & -U^2 C_{21} & 2\beta U B_{21} \\ 0 & 0 & 0 & 1 \\ -U^2 C_{12} & 2\beta U B_{12} & -\Omega_2^2 - U^2 C_{22} & 2\beta U B_{22} - A_1 \varsigma \end{bmatrix} \begin{Bmatrix} q_1 \\ p_1 \\ q_2 \\ p_2 \end{Bmatrix} + f(p_1, p_2), \tag{32}$$

where $f(p_1,p_2)$ is a vector containing the nonlinear terms. The complex eigenvalues of the system linearized about the equilibrium (there is only one, at the origin of the phase space) are plotted in Fig. 8 for increasing values of U. Similarly to the one-mode approximation, the instability occurs through the Hopf bifurcation, leading to flutter. Using again the base case parameters (Table 1), the critical velocity for the two-mode approximation is equal to $U_{\text{crit}} = 4.45$, which is approximately half of the value for the one-mode approximation. To understand this significant reduction in critical flow velocity, an energy analysis is performed for the two-mode approximation. At the critical velocity the solution of the equation of motion, using the two-mode approximation, can be written as

$$\eta(\xi, \tau) = \sum_{m=1}^{2} \phi_m(\xi) q_m(\tau) = \phi_1(\xi) \hat{q}_1 \cos(\omega_2 \tau) + \phi_2(\xi) \hat{q}_2 \cos(\omega_2 \tau - \alpha), \tag{33}$$

where ω_2 is the dimensionless frequency with which modes 1 and 2 vibrate (it is the only real frequency) and α is the phase lag between modes 1 and 2. In this analysis, only the pair of pure imaginary eigenvalues is taken into account, since the contribution of the other two complex eigenvalues vanishes quickly with time. Using the two-mode solution, Eq. (33), the contributions to the energy loss over one period given by the centrifugal force, the Coriolis force and the linear part of the hydrodynamic drag are now equal to, respectively:

$$\begin{aligned} \Delta E_{\text{Cent.}} &= \int_0^T \int_0^1 F_{\text{Cent.}} \frac{\partial \eta}{\partial \tau} \, \mathrm{d}\xi \, \mathrm{d}\tau = U_{\text{crit}}^2 \int_0^T \int_0^1 \left(\frac{\mathrm{d}^2 \phi_1}{\mathrm{d}\xi^2} q_1 + \frac{\mathrm{d}^2 \phi_2}{\mathrm{d}\xi^2} q_2 \right) \left(\phi_1 \frac{\mathrm{d}q_1}{\mathrm{d}\tau} + \phi_2 \frac{\mathrm{d}q_2}{\mathrm{d}\tau} \right) \mathrm{d}\xi \, \mathrm{d}\tau \\ &= U_{\text{crit}}^2 \pi \hat{q}_1 \hat{q}_2 \sin(\alpha) \int_0^1 \left(\frac{\mathrm{d}^2 \phi_1}{\mathrm{d}\xi^2} \phi_2 - \frac{\mathrm{d}^2 \phi_2}{\mathrm{d}\xi^2} \phi_1 \right) \mathrm{d}\xi, \end{aligned} \tag{34}$$

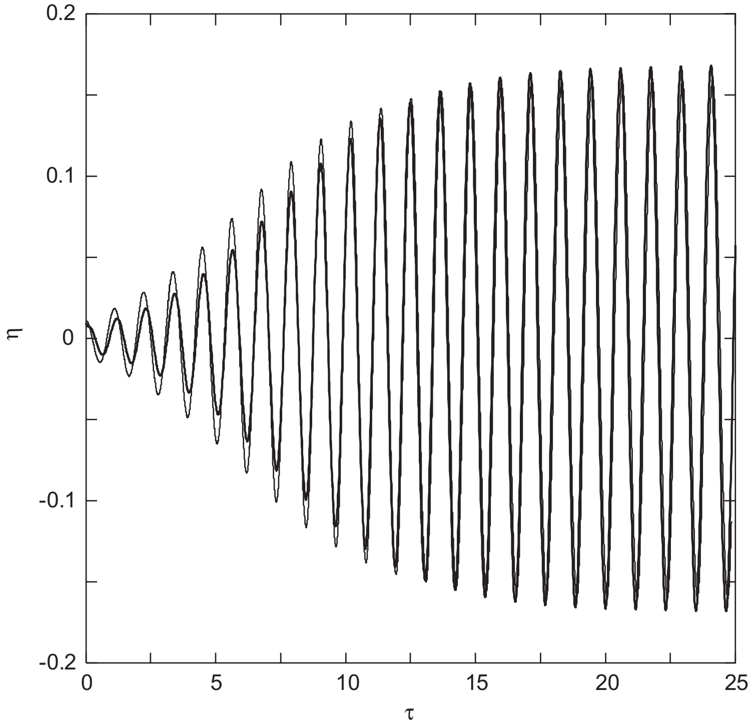

Fig. 9. Comparison of tip deflections using 12 mode approximation (regular line) and finite difference method (bold line).

$$\Delta E_{\mathrm{Cor.}} = \int_0^T \int_0^1 F_{\mathrm{Cor.}} \frac{\partial \eta}{\partial \tau}\, \mathrm{d}\xi\, \mathrm{d}\tau = -2\beta U_{\mathrm{crit}} \int_0^T \int_0^1 \left(\frac{d\phi_1}{d\xi}\frac{dq_1}{d\tau} + \frac{d\phi_2}{d\xi}\frac{dq_2}{d\tau} \right) \left(\phi_1 \frac{dq_1}{d\tau} + \phi_2 \frac{dq_2}{d\tau} \right) d\xi d\tau$$
$$= -2\beta U_{\mathrm{crit}} \pi\omega \int_0^1 \left(\frac{\mathrm{d}\phi_1}{\mathrm{d}\xi}\, \phi_1 \hat{q}_1^2 + \left(\frac{\mathrm{d}\phi_1}{\mathrm{d}\xi}\, \phi_2 + \frac{\mathrm{d}\phi_2}{\mathrm{d}\xi}\, \phi_1 \right) \hat{q}_1 \hat{q}_2 \cos(\alpha) + \frac{\mathrm{d}\phi_2}{\mathrm{d}\xi}\, \phi_2 \hat{q}_2^2 \right) \mathrm{d}\xi, \tag{35}$$

$$\Delta E_{\mathrm{DragL.}} = \int_0^T \int_0^1 F_{\mathrm{Drag}L.} \frac{\partial \eta}{\partial \tau}\, \mathrm{d}\xi\, \mathrm{d}\tau = A_1 \varsigma \int_0^T \int_0^1 \left(\phi_1 \frac{\mathrm{d}q_1}{\mathrm{d}\tau} + \phi_2 \frac{\mathrm{d}q_2}{\mathrm{d}\tau} \right)^2 \mathrm{d}\xi\, \mathrm{d}\tau$$
$$= A_1 \varsigma \pi \omega \int_0^1 (\phi_1^2 q_1^2 + \phi_2^2 q_2^2)\, \mathrm{d}\xi. \tag{36}$$

Using Eq. (24), it can be shown that the remaining terms in the equation of motion, Eq. (22), do not contribute to the energy variation over one period. In contrast to the one-mode approximation, the centrifugal force contributes to the energy variation in the two-mode approximation. Whether this force leads to energy loss or energy gain depends on the value of the phase shift α between the two modes. Using the parameters in Table 1, the energy expression for the centrifugal force, Eq. (34), is negative, implying an energy gain. The energy gain caused by the centrifugal force is of the same order as caused by the Coriolis force. The additional contribution of the centrifugal force results in a reduction of the critical velocity with almost a factor of 2 with respect to the one-mode approximation.

Using the two-mode approximation, the behaviour of the cantilever pipe after the onset of flutter has been analysed by incorporating the full nonlinear equation, Eq. (32). As expected, for a fluid velocity exceeding the critical one, a stable limit cycle arises in the four-dimensional phase space (not shown).

5.4. Multi-mode approximation

In order to achieve a sufficient accuracy with the Galerkin method, more than two modes should be taken into account. It appears that for this system twelve modes are sufficient, since by incorporating more modes the response of the pipe hardly changes. For the pipe of 2 m length and the parameters given in Table 1, the dimensionless critical velocity is 4.40, which is only slightly less than computed with the two-mode approximation. The 12-mode approximation is compared with a numerical method employing a central, explicit finite difference scheme. This comparison is shown in Fig. 9. The displacement of the tip of the pipe is plotted in the time domain after the system is released from an initial deflection for an internal fluid velocity just exceeding the critical one. Fig. 9 shows good correspondence between predictions of the two methods. The difference in the transient regime is caused by slightly different initial conditions used in the computations.

After analysing the one-, two- and twelve-mode approximations the following can be concluded:

(i) A one-mode approximation describes the physical behaviour of the system incorrectly since in this approximation the centrifugal force does not contribute to the energy variation in the system.
(ii) A two-mode approximation describes the dynamic behaviour of the system qualitatively correctly. Even in a quantitative sense this is a reasonable approximation.
(iii) Both the centrifugal and Coriolis forces contribute to the energy gain of the free-hanging pipe conveying fluid.

6. Conclusion

Experiments with cantilever pipes aspirating water up to now never showed any instability. Using the new tip boundary conditions proposed by Païdoussis et al. (2005), Eq. (10), the simulated pipe of 2 m length is predicted to become unstable by divergence at a dimensionless flow velocity $U_{\text{crit}} = 1.59$. This corresponds to a fluid velocity of $u_{f,\text{crit}} = 4.53\,\text{m/s}$. It is far from easy to achieve such high internal fluid speeds in a pipe of 0.03 m diameter, and hence, it is not surprising that the experiments did not show any instability.

Using the theory proposed in this paper, which assumes that the momentum of the fluid does not change direction as the fluid enters the pipe, in combination with a realistic description of the hydrodynamic drag, the cantilever pipe is predicted to become unstable at $U_{\text{crit}} = 4.40$, corresponding to a fluid speed of $u_{f,\text{crit}} = 12.6\,\text{m/s}$. It is impossible to achieve such high internal fluid speeds in a 0.03 m diameter pipe. Hence, in our view theory and experiments do not show any contradiction.

Probably, the truth will not be described by just one of the two discussed theories. We expect that an intermediate approximation is more likely. Both the correct description of the flow field in the vicinity of the tip and the external hydrodynamic drag will be of great importance for the prediction of the stability of the pipe conveying fluid. For this reason we initiated new experiments using longer pipes, so that the critical velocity becomes attainable. The experiments will hopefully reveal whether and how the pipe becomes unstable, i.e. by divergence or by flutter, and at which internal fluid velocity.

Acknowledgements

This research is supported by the Technology Foundation STW, Applied Science Division of NWO and the technology programme of the Ministry of Economic Affairs.

References

Bearman, P.W., Mackwood, P.R., 1992. Measurements of the hydrodynamic damping of circular cylinders. In: Proceedings of the Sixth International Conference on the Behavior of Offshore Structures (BOSS '92), London, pp. 405–414.

Bearman, P.W., Russell, M.P., 1996. Measurements of the hydrodynamic damping of bluff bodies with application to the prediction of viscous damping of TLP hulls. In: Proceedings of the 21st Symposium on Naval Hydrodynamcis, Washington, DC, USA, pp. 622–634.

Chaplin, J.R., 2000. Hydrodynamic damping of a cylinder at $\beta \approx 10^6$. Journal of Fluids and Structures 14, 1101–1117.

Chaplin, J.R., Subbiah, K., 1998. Hydrodynamic damping of a cylinder in still water and in a transverse current. Applied Ocean Research 20, 251–259.

Justesen, P., 1988. Hydrodynamic forces on large cylinders in high Reynolds number oscillatory flow. BOSS Conference, 805–819.

Kuiper, G.L., Metrikine, A.V., 2005. Dynamic stability of a submerged, free hanging riser conveying fluid. Journal of Sound and Vibration 280, 1051–1065.

Lee, S.-Y., Mote, C.D., 1997. A generalized treatment of the energetics of translating continua, Part II: Beams and fluid conveying pipes. Journal of Sound and Vibration 204, 735–753.

Païdoussis, M.P., 1998. Fluid–Structure Interactions: Slender Structures and Axial Flow, vol. 1. Academic Press, London.

Païdoussis, M.P., 1999. Aspirating pipes do not flutter at infinitesimally small flow. Journal of Fluids and Structures 13, 419–425.

Païdoussis, M.P., Luu, T.P., 1985. Dynamics of a pipe aspirating fluid, such as might be used in ocean mining. ASME Journal of Energy Resources Technology 107, 250–255.

Païdoussis, M.P., Semler, C., Wadham-Gagnon, M., 2005. A reappraisal of why aspirating pipes do not flutter at infinitesimal flow. Journal of Fluids and Structures 20, 147–156.

Rodenbusch, G., Kallstrom, C., 1986. Forces on a Large Cylinder in Random Two-dimensional Flow. OTC, Houston.

Sarpkaya, T., 1986. Force on circular cylinder in viscous oscillatory flow at low Keulegan–Carpenter numbers. Journal of Fluid Mechanics 165, 61–71.

Sarpkaya, T., 2001. Hydrodynamic damping and quasi-coherent structures at large Stokes numbers. Journal of Fluids and Structures 15, 909–928.

Stokes, G.G., 1851. On the effect of the internal friction fluids on the motion of pendulums. Transactions of Cambridge Philosophical Society 9, 8–106.

Wang, C.-Y., 1968. On high frequency oscillating viscous flows. Journal of Fluid Mechanics 32, 55–68.